Supporting Information

Highly stable Mn-Sn flow batteries towards low-temperature energy storage

Yu Shu[†a], Yexuan Yu,[†a] Hongjie Xiao,[a] Ziyi Xiang,[a] Liping Wan,[a] Guodong Li,[b] Yao Liu,[c] Jianhang Huang,[*a] Yonggang Wang[*b]

[a] Key Laboratory of the Ministry of Education for Advanced Catalysis Materials, Zhejiang Key Laboratory of Advanced Catalysis and Adsorption Materials, College of Chemistry and Materials Science, Zhejiang Normal University, Jinhua 321004, China.

[b] Department of Chemistry and Shanghai Key Laboratory of Molecular Catalysis and Innovative Materials, iChEM (Collaborative Innovation Center of Chemistry for Energy Materials), Fudan University, Shanghai 200433, China.

[c] Shanghai Institute of Applied Physics, Chinese Academy of Sciences, Shanghai, 201800, China

[†] Both parties have made comparable contributions to this paper.

Method details

Chemicals and materials

Manganese sulfate ($MnSO_4$, AR), titanium sulfate ($Ti(SO_4)_2$, CP), sulfuric acid (H_2SO_4, AR) were purchased from Sinopharm Chemical Reagent Co., Ltd. Tin sulfate ($SnSO_4$, AR) and tin sheet were received from Aladdin and Sinopharm Chemical Reagent Co., Ltd, respectively. Gelatin (GEL, CP) was received from Xilong Chemical Co., Ltd. Carbon felt and flexible graphite plate were received from Nake New Materials Co., Ltd. PBI membrane was received from Zhongke Energy Materials Technology (Dalian) Co., Ltd. Nafion membrane (N212, Dupont) was received from Dupont China Group Co., Ltd.

Material characterization

Scanning electron microscope (SEM) images were acquired from a field emission scanning electron microscope (ZEISS Gemini SEM 300, Germany). XRD patterns were recorded by X-ray diffractometer (D8 Advance from Bruker AXS), using the monochromatic Cu Kα line as the radiation source (λ = 0.15406 nm). Raman spectra were collected using a Via-Refler instrument from Reninshaw under the condition of a 532 nm laser. Attenuated total reflectance-Fourier transform infrared (ATR FTIR) spectra of the electrolyte were collected using a Nicolet 6700 FT-IR spectrometer. X-ray Absorption Fine Structure (XAFS) was collected in the transmission mode using an in-house laboratory-based X-ray absorption spectrometer (SuperXAFS M9000)[63]. Differential Scanning Calorimetry (DSC) was collected in NETZSCH DSC 200F3 in the procedure from 25 °C to −100 °C with a Cooling rate of 1 $K \cdot min^{-1}$.

Electrochemical measurement

Cyclic voltammetry (CV) was carried out using a three-electrode system. For the Mn^{2+}/Mn^{3+} chemistry, a graphite plate was used as the working electrode, carbon felt as the counter electrode, and a calomel electrode as the reference electrode. For the CV of Sn^{2+}/Sn chemistry, Cu was used as the working electrode, Sn as the counter electrode, and a calomel electrode as the reference electrode. The above CVs were all used SP-300 electrochemical workstation (Bio-Logic, France) under a scan rate from 5 $mV \cdot s^{-1}$ to 25 $mV \cdot s^{-1}$. For the galvanostatic Sn deposition/dissolution test in a Cu/Sn asymmetric battery, a classic two-electrode system was constructed using an electrolyte containing a GEL additive. In this system, a commercial copper foam (3 mm, 60 ppi) was selected as the working electrode, a Sn foil was used as the counter electrode and reference electrode, and the tests were carried out under the condition of magnetic stirring (aiming to simulate the flow state of the electrolyte in a flow battery).

Conductivity measurements

Using an SP-300 electrochemical workstation (Bio-Logic, France), the conductivity of the electrolytes was measured via the A.C. impedance method. The calculation formula for ionic conductivity is as follows:

$$\sigma_{ion} = \frac{L}{AR}$$

Where σ_{ion} is the ionic conductivity, R is the AC impedance value. L is the distance between the two parallel electrode sheets, while A is the area of the electrode sheets.

Theoretical calculations

MD simulations were performed to study hydrogen bonding in three aqueous solutions: pure water, 1M $MnSO_4$ + 1M $Ti(SO_4)_2$ + 3M H_2SO_4, and 0.2M $SnSO_4$ + 5M H_2SO_4. Simulations utilized the Forcite module with the Universal force field. The pure water model consisted of 500 H_2O molecules. The 1M $MnSO_4$ + 1M $Ti(SO_4)_2$ + 3M H_2SO_4 model was constructed using the Amorphous Cell module by adding nine Mn^{2+} ions, nine Ti^{4+} ions, and fifty-four SO_4^{2-} ions to 500 H_2O molecules. Similarly, the 0.2M $SnSO_4$ + 5M H_2SO_4 model was built by adding two Sn^{2+} ions, ninety H^+ ions, and forty-seven SO_4^{2-} ions to 500 H_2O molecules. Before MD simulations, the geometry of each solution model was optimized using ultra-fine quality settings. Subsequently, NVT ensemble simulations were conducted at 298.15 K for 2000 ps. Data analysis focused on the final 1000 ps of each NVT trajectory. Hydrogen bonds were identified based on geometric criteria: an H···O distance between 1.0 Å and 3.1 Å, and an O–H···O angle between 90° and 180°. Hydrogen bond analysis was performed using a custom Perl script implementing these criteria.

Determination of the diffusion coefficient

For a reversible system, the peak current follows a linear relationship with the square root of the scan rate. The Randles-Sevcik equation can be used to solve for D:

$$Slope = 2.69 \times 10^5 n^{3/2} A C^* D^{1/2}$$

In the formula, n is the number of electrons, A is the electrode geometric area, C^* is the bulk concentration, and D is the diffusion coefficient.

Flow cell measurements

The home-made flow battery with an effective area of 10 cm^2 was assembled at room temperature. PBI separator placed between two carbon felts (thickness 5 mm), which were in contact with the serpentine flow channel graphite plate as current

collector. To avoid liquid leakage between components, a fluorine rubber pad was used for sealing treatment. The electrolytes were pumped in by a peristaltic pump (Nanjing Runze Fluid Control Equipment Co., Ltd.), at a flow rate of 70 $mL \cdot min^{-1}$. The structure of the low-temperature battery was the same as that of the room-temperature battery, and the separator can be N212. The N212 separator needed to be pre-soaked in 3 M H_2SO_4 for 30 minutes. It is particularly pointed out that during the low-temperature battery testing process, except for the circuit controller, all components (including the battery, electrolyte, peristaltic pump, and pipelines etc.) were placed in a low-temperature chamber to guarantee a reliable and accurate low-temperature environment (Figure S38). The dosage of the positive electrode electrolyte was set at 10 mL, and the capacity provided by the anolyte was 3 times the capacity of the catholyte. For all room temperature MSFB tests, 0.2 M $SnSO_4$ + 3 M H_2SO_4 + 1 g L^{-1} GEL were used as the anolyte. In all low-temperature tests, 0.2 M $SnSO_4$ + 5 M H_2SO_4 + 1 g L^{-1} GEL was used as anolyte. To accurately measure the battery power, a polarization test was carried out at a state of charge (SOC) was 80%. During the test, the scanning rate was set at 100 mV s^{-1}, and the voltage range was controlled between 1.75 − 0.6 V. The large-sized battery mold in Figure S35 is provided by Wuhan Zhisheng New Energy Co., Ltd.

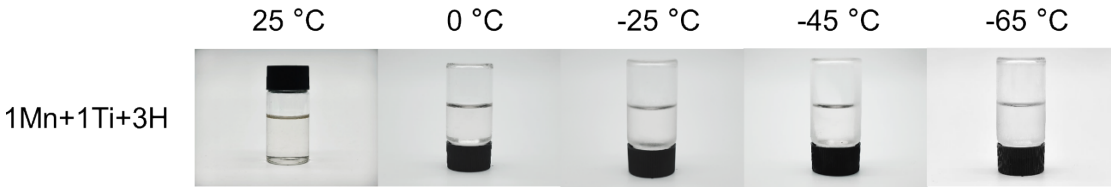

Figure S1. Optical photos of the cathode electrolyte at different temperatures. It can be seen that even at −65 °C, the electrode liquid remains flowing.

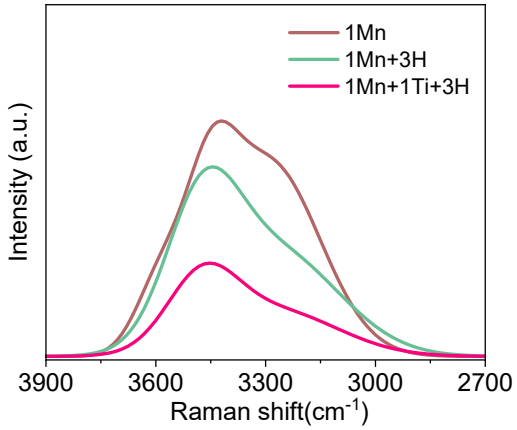

Figure S2. The Raman spectra of the catholyte of 1 Mn, 1 Mn + 3 H, and 1 Mn + 1 Ti + 3 H.

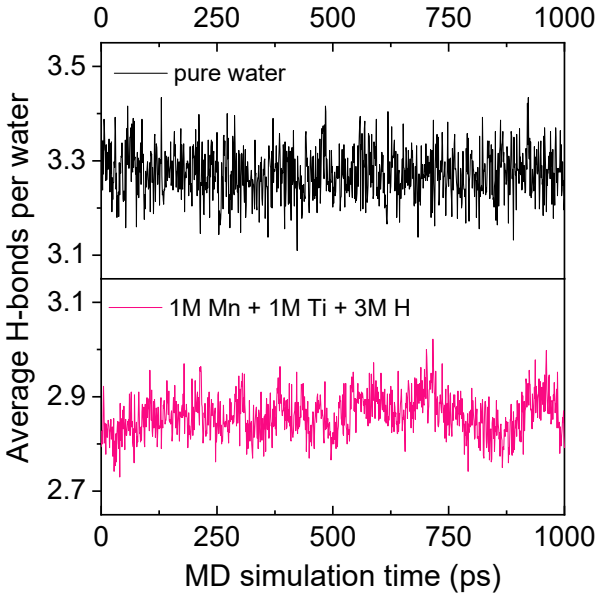

Figure S3. MD simulation calculation of the average number of H-bonds in pure water and the designed catholyte (1 Mn + 1 Ti + 3 H).

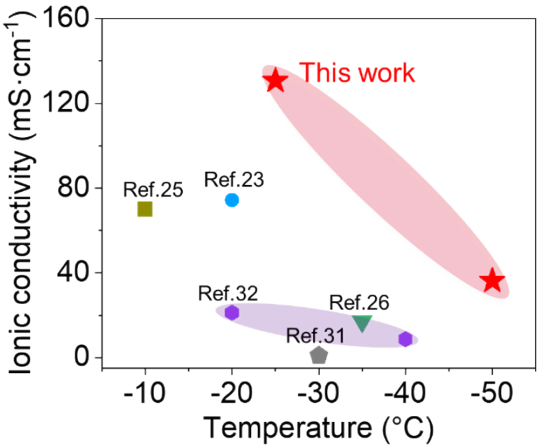

Figure S4. Comparison of ionic conductivity at low temperature between this work and previously published work.

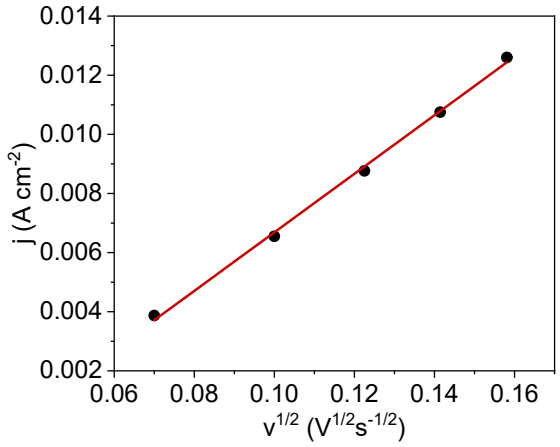

Figure S5. The diffusion coefficient of the Mn catholyte at 25 °C. It is calculated from the square root of the scan rate and the reduction peak current density.

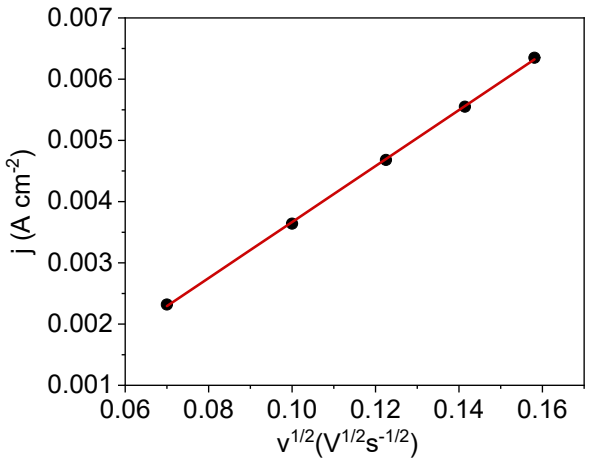

Figure S6. The diffusion coefficient of the Mn catholyte at −45 °C.

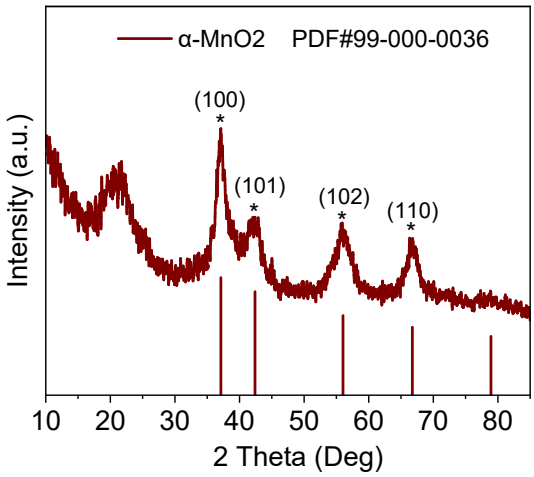

Figure S7. XRD pattern of insoluble MnO_2 formed on the surface of carbon felts.

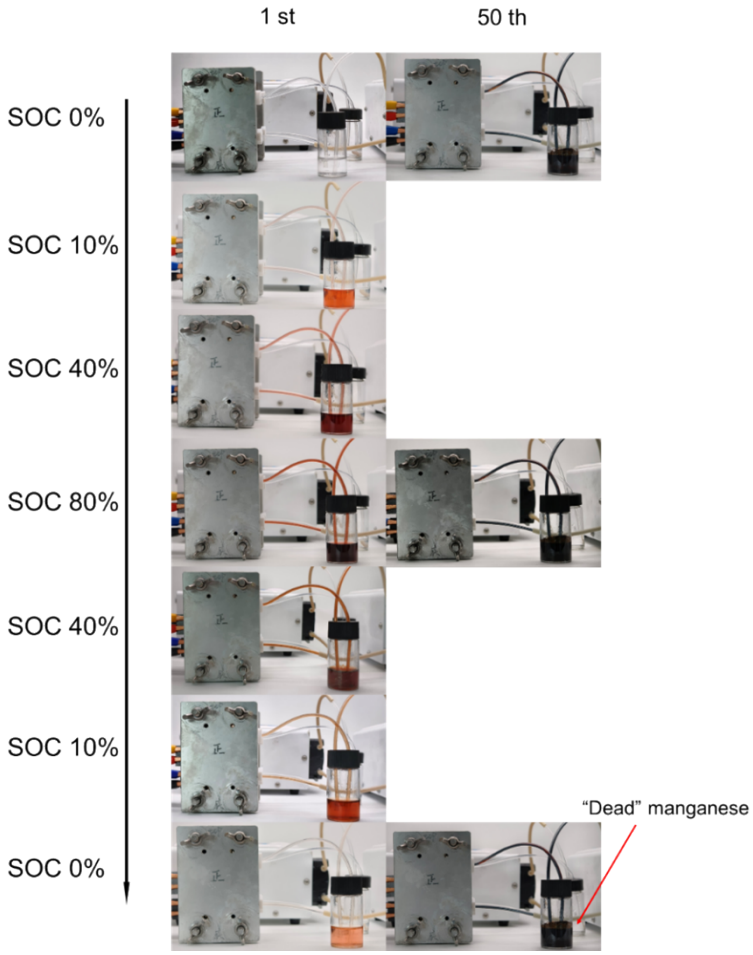

Figure S8. The optical photos of the battery assembled with 0.2 Mn + 3 H as the catholyte at the 1st and 50 th. There is still a large amount of dead manganese in the solution after 50 th at the end of discharge.

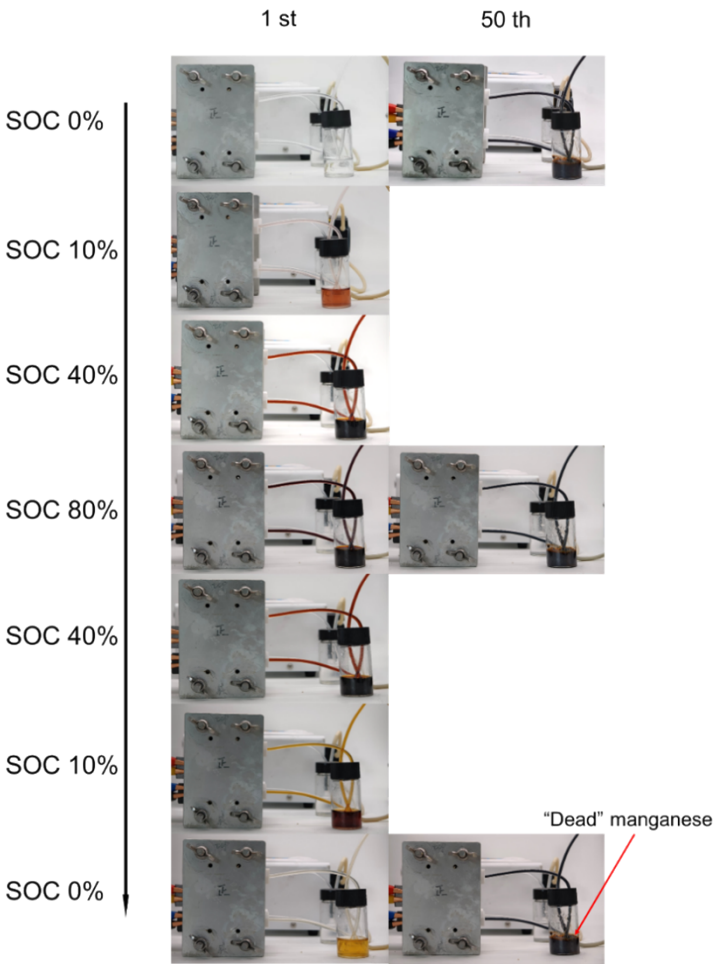

Figure S9. The optical photos of the battery assembled with 0.2 Mn + 0.4 Ti as the catholyte at the 1st and 50 th. There is also a large amount of dead manganese in the solution after 50 th at the end of discharge.

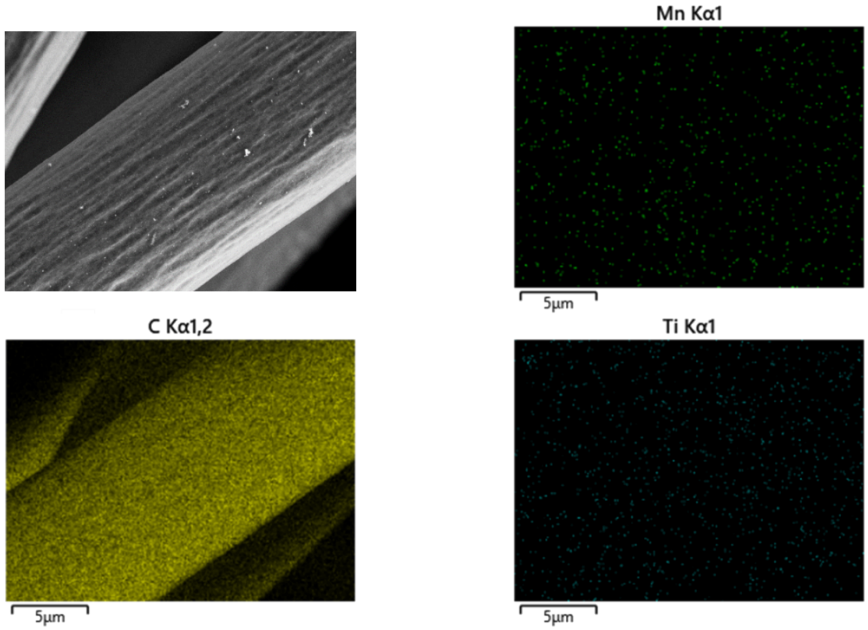

Figure S10. SEM images and elemental mappings (Mn, C, Ti) of the carbon felt of the battery assembled with 0.2 Mn + 0.4 Ti + 3 H as the catholyte after 3000 cycles. No obvious “dead manganese” particles were observed on the surface of the carbon felt.

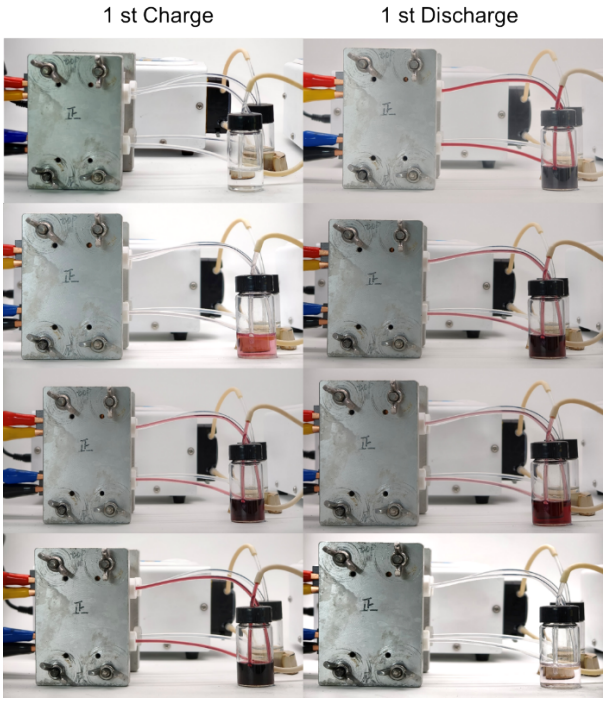

Figure S11. The optical photos of the battery assembled with 0.2 Mn + 0.4 Ti + 3 H as the catholyte at the 1 st.

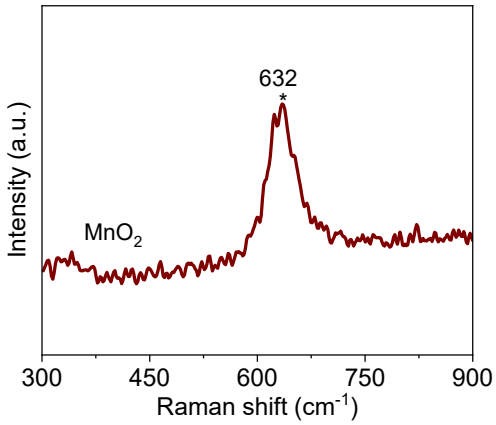

Figure S12. The Raman spectra of MnO_2 exhibit distinct double peaks at 632 cm^{-1}.

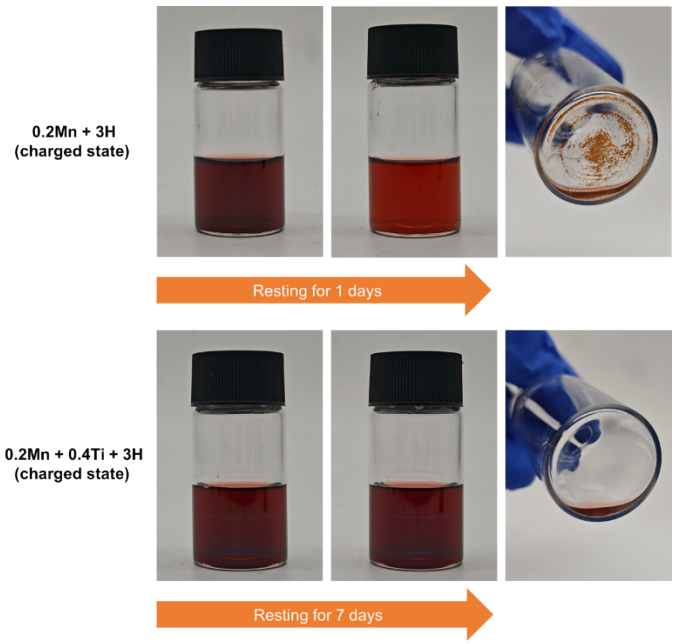

Figure S13. The comparison of the stability for the electrolytes with and without titanium ions in the charged state. It can be seen that after standing for one day, the color of the 0.2Mn + 3H electrolyte (charged state) became lighter, which is attributed to the disproportionation of trivalent manganese, accompanied by the obvious formation of manganese dioxide. While the color of the 0.2Mn + 0.4Ti + 3H electrolyte (charged state) has no change after 7 days of standing, and there is no precipitation formed, indicating that trivalent manganese can be stabilized by the titanium ions.

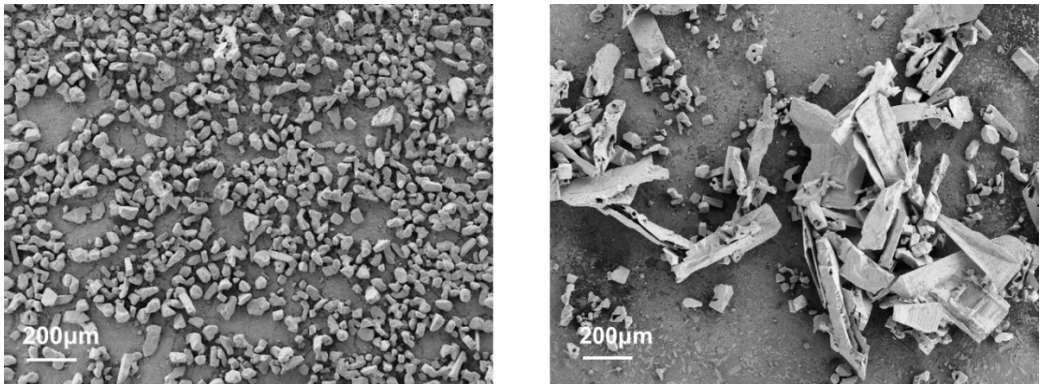

Figure S14. Deposition morphology of Sn particles under deposition capacity of 5 mA with 5 mAh·cm^{-2}. From left to right are: 0.2 Sn + 3 H + GEL electrolyte, 0.2 Sn + 3 H electrolyte, respectively.

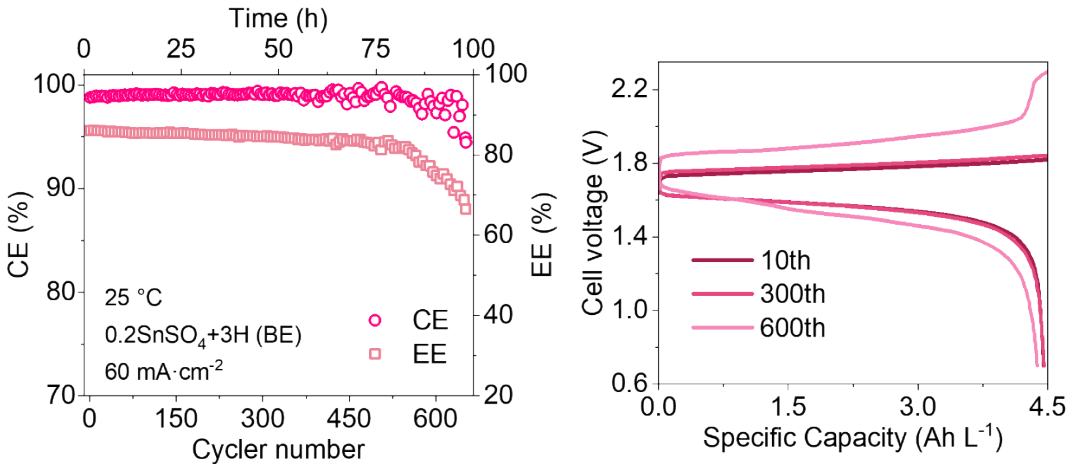

Figure S15. The overall cycling performance and charge-discharge curves of the MSFB using 0.2 $SnSO_4$ + 3 H without GEL at 60 mA·cm^{-2}.

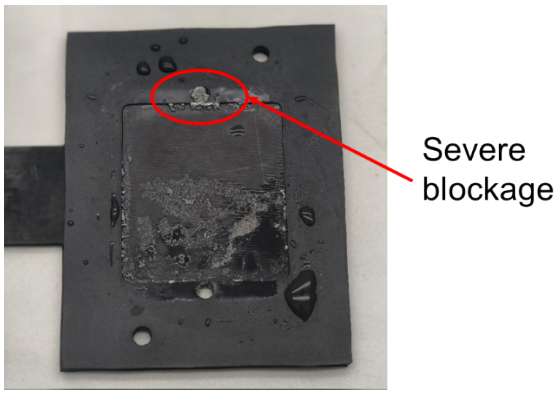

Figure S16. During the cycling process of the MSFB assembled with 0.2 Sn + 3 H, dead tin blocked the flow channel.

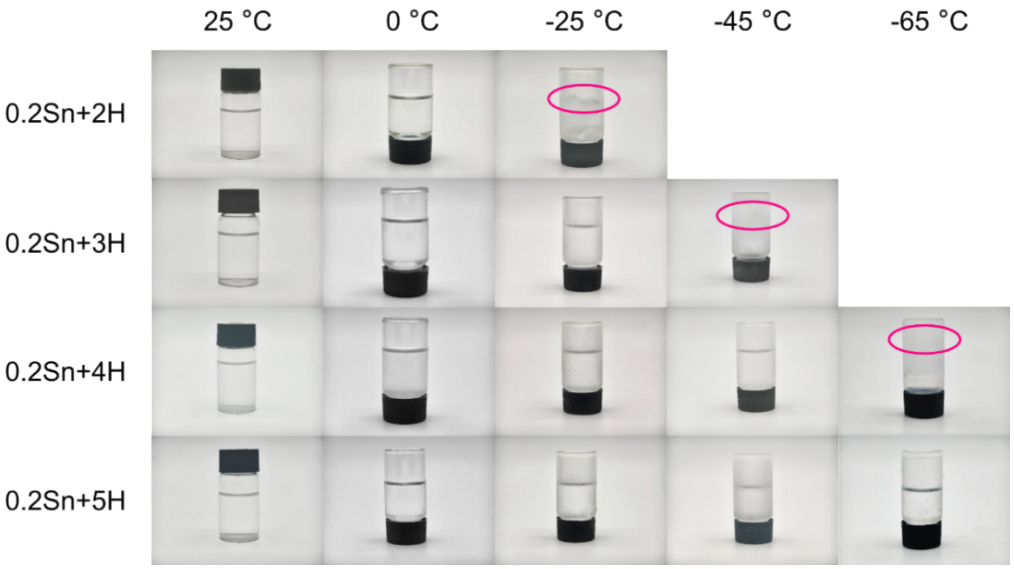

Figure S17. Digital photos of anolyte with different compositions from −65°C to 25°C. An electrolyte containing 5 mol H can remain flowing at −65 °C.

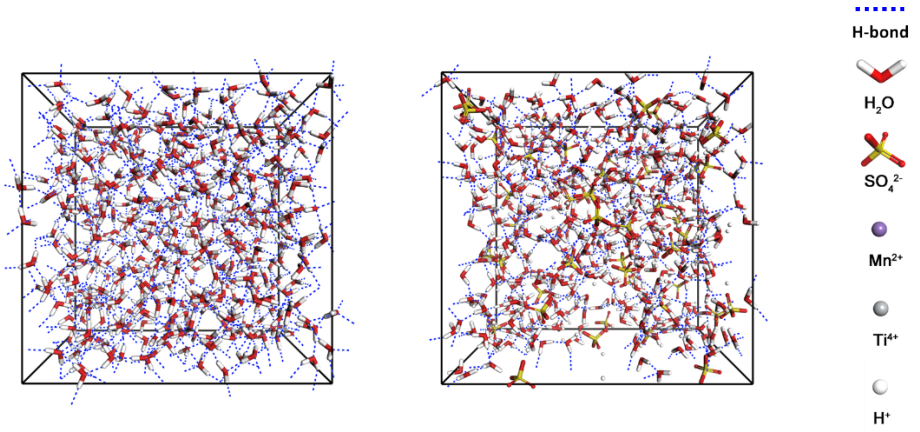

Figure S18. MD simulation snapshots of pure water (left) and the anolyte (right).

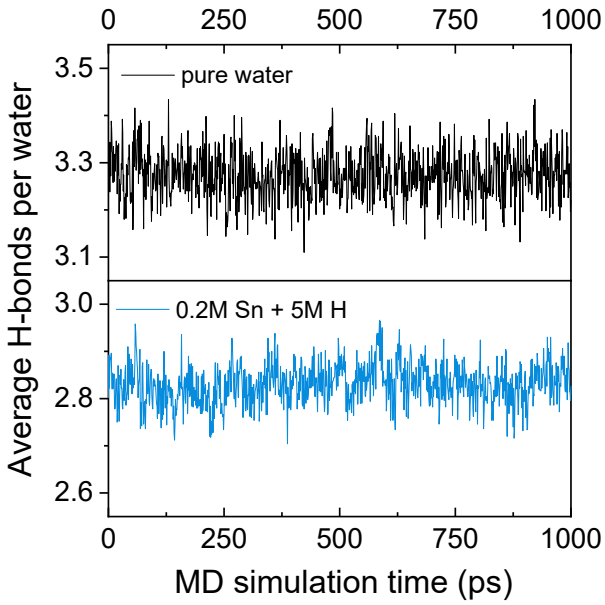

Figure S19. MD simulation calculation of the average number of H-bonds in pure water and the designed anolyte (0.2 Sn + 5 H).

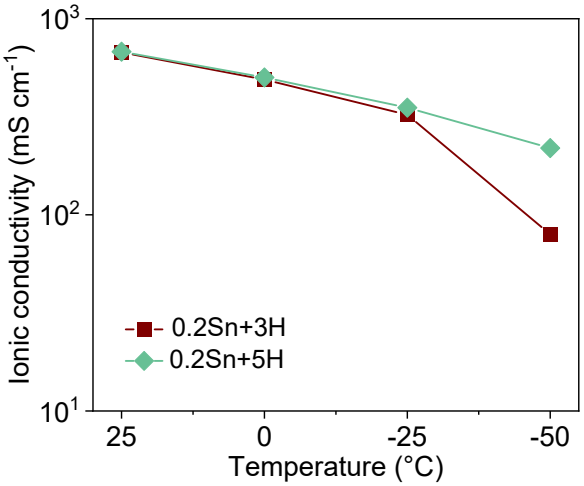

Figure S20. Ionic conductivity of different anolytes from 25 to −50 °C.

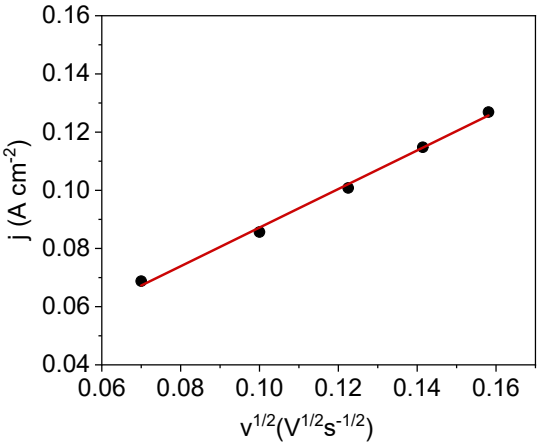

Figure S21. The diffusion coefficient (1.9×10^{-5} cm^2 s^{-1}) of the Sn anolyte at 25 °C.

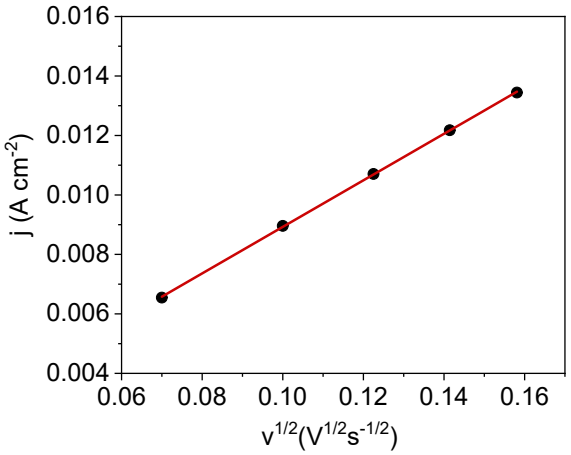

Figure S22. The diffusion coefficient of the Sn anolyte at −45 °C.

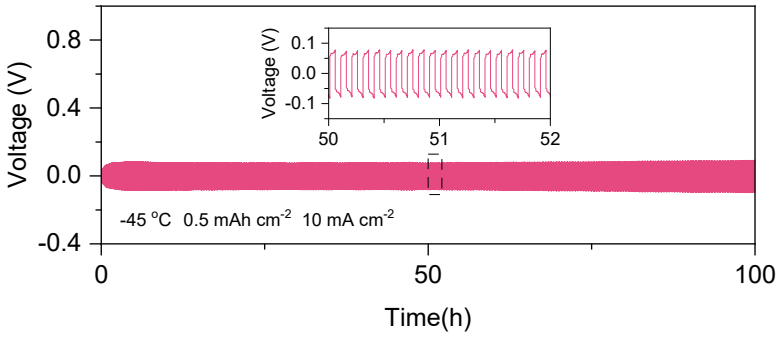

Figure S23. Cycle performance of Sn-Sn symmetrical flow battery with 0.2 M $SnSO_4$ + 5 M H_2SO_4 + 1 g L^{-1} GEL electrolyte and Nafion 212 membrane at −45°C. It shows stable charge/discharge polarization of 126 mV, which shows high reversibility of Sn anolyte.

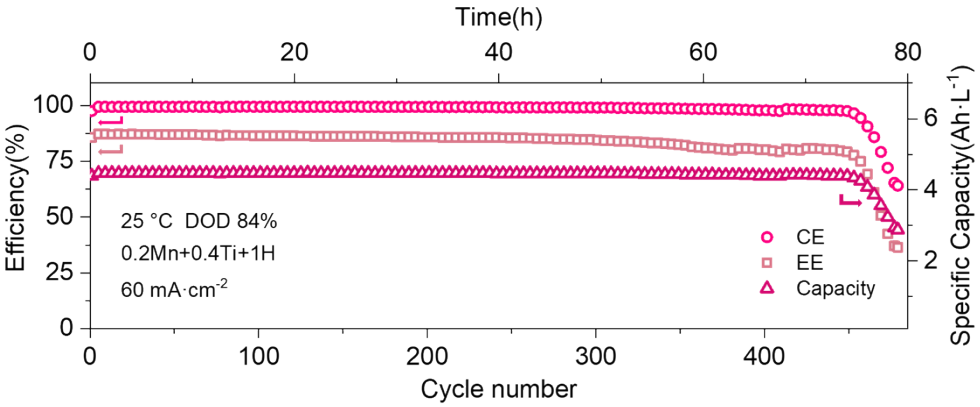

Figure S24. The overall cycling performance of the MSFB (0.2Mn + 0.4Ti + 1H) with a DOD of 84% (single electron) at 60 mA·cm^{-2}. The cycling performance of the battery with low concentration acid electrolytes showed a rapid capacity decay after 450 cycles. In contrast, the 0.2Mn + 0.4Ti + 3H electrolyte can achieve over 5000 cycles. Given that reducing the acid concentration severely affects the cycling performance of the positive electrolyte, we adopted the 3 M acid electrolyte.

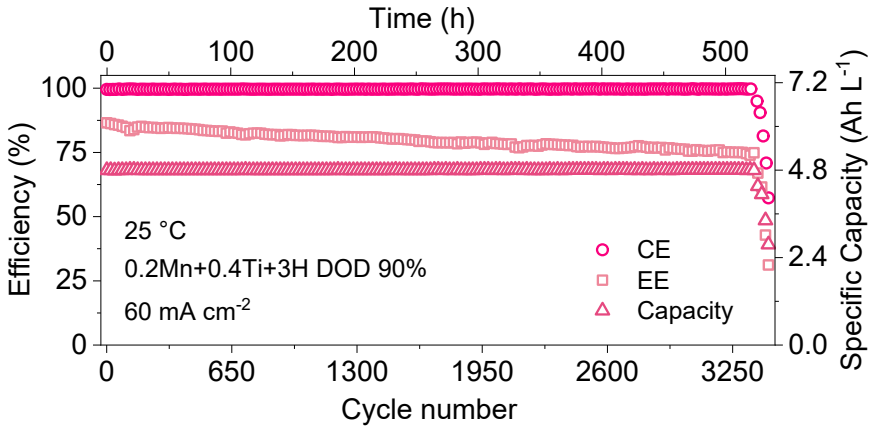

Figure S25. The overall cycling performance of the MSFB with a DOD of 90% (single electron) at 60 mA·cm^{-2}.

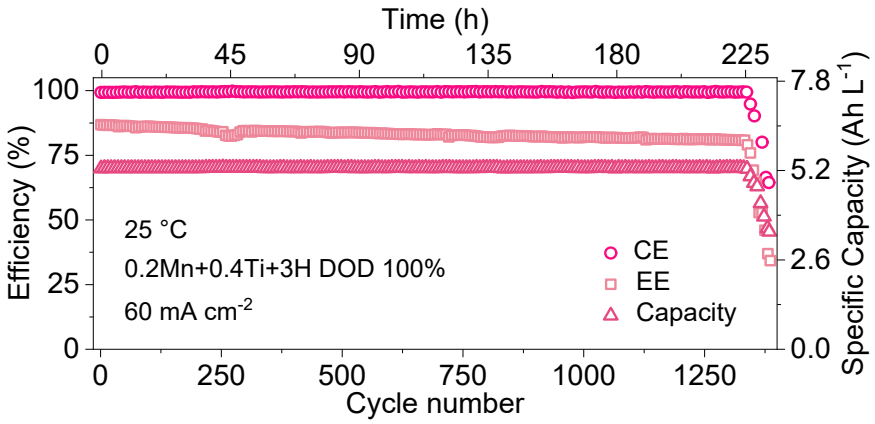

Figure S26. The overall cycling performance of the MSFB with a DOD of 100% (single electron) at 60 mA·cm^{-2}.

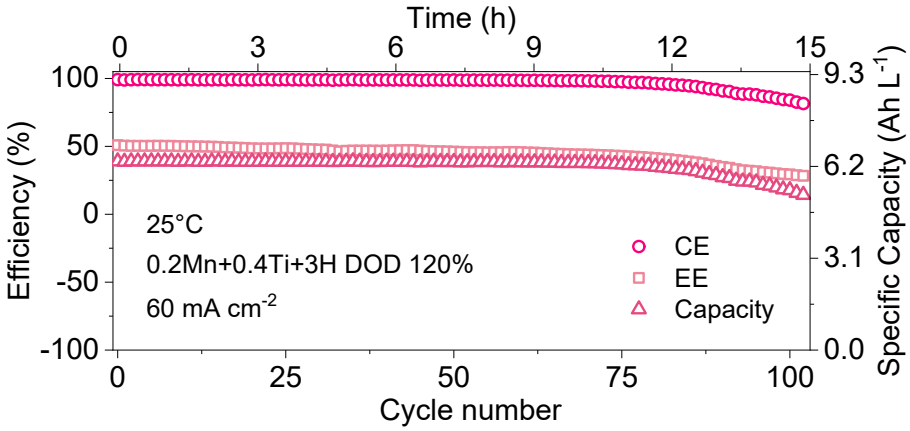

Figure S27. The overall cycling performance of the MSFB with a DOD of 120% (single electron) at 60 mA·cm^{-2}.

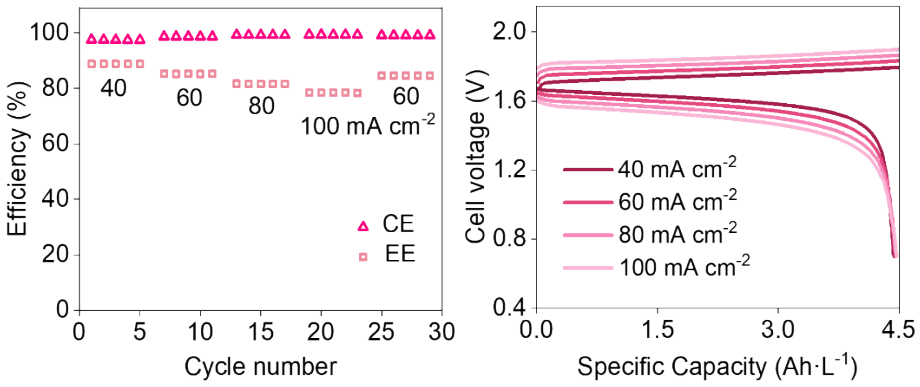

Figure S28. Rate performance and charge-discharge curves of 0.2 Mn + 0.4 Ti + 3 H at various current densities, the discharge process ended with a cutoff voltage of 0.7 V.

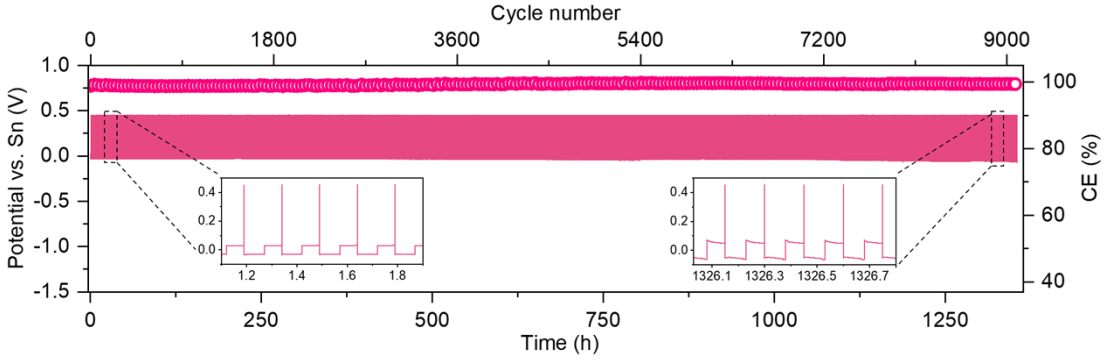

Figure S29. Coulombic efficiency and voltage profiles of Sn plating/stripping in Sn//Cu foam asymmetrical cells evaluated at 60 mA·cm^{-2} with 4.5 mAh·cm^{-2} at 25 °C.

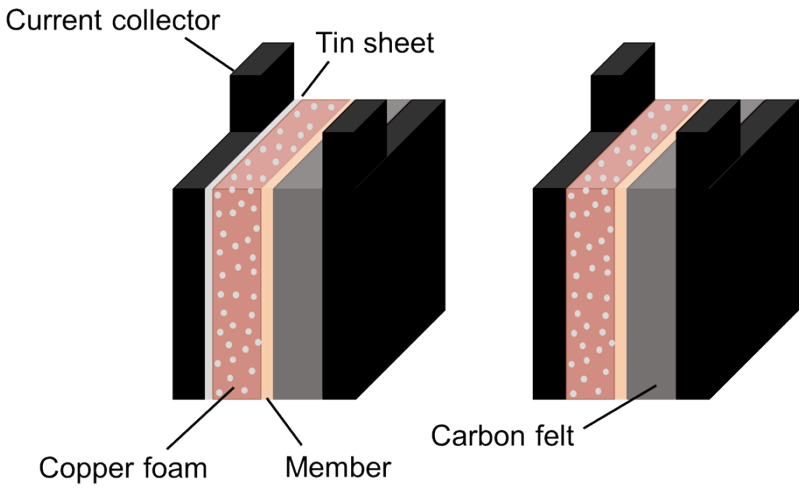

Figure S30. Schematic diagrams of the internal structures of conventional batteries (left) and dual-electrode-free batteries (right).

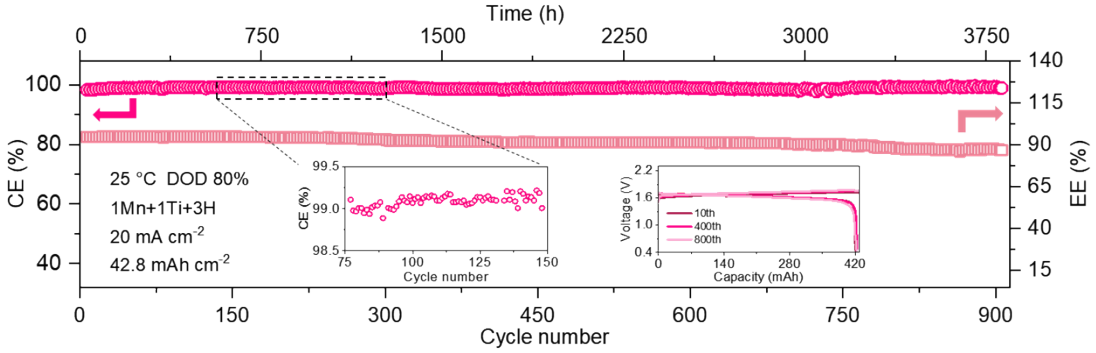

Figure S31. Long-term cycling performance of the MSFB using concentrated 1Mn + 1Ti + 3H and N212 membrane at 20 mA·cm^{-2}.

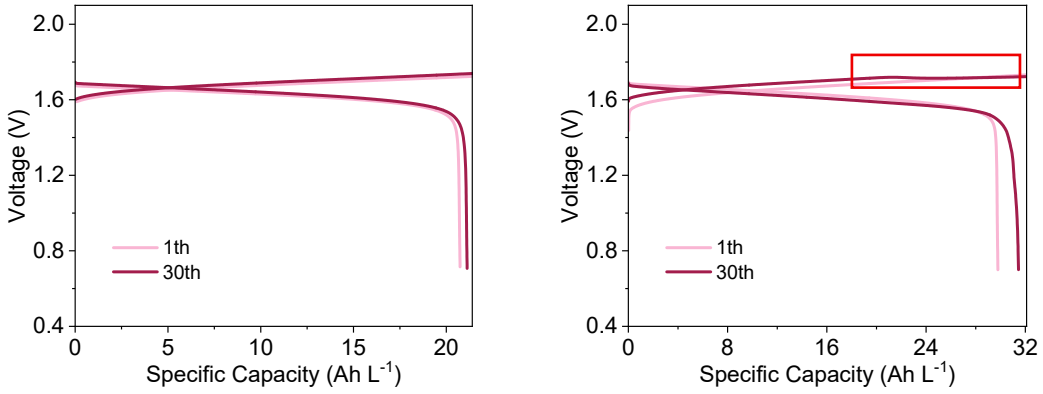

Figure S32. Charge-discharge curves of Catholyte with different concentrations at different numbers of cycles. During the charge-discharge process of the battery using the 1 Mn + 1 Ti + 3 H solution (left side), only polarization changes occurred. For the battery using the 1.5 Mn + 1.5 Ti + 3 H solution (right side), a charging plateau of MnO_2 appeared in the 30 th cycle.

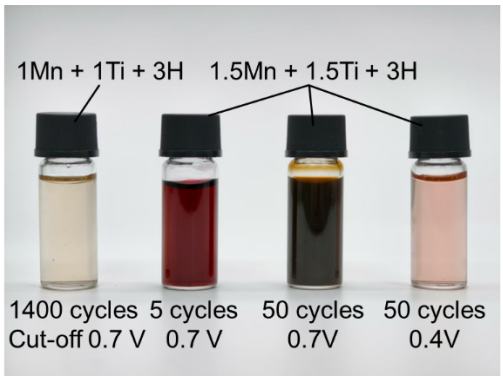

Figure S33. Optical photos of the discharged state of different electrolytes at 25 °C under different cut-off voltages. From left to right, they are as follows: 1 Mn + 1Ti + 3H after 1400 cycles (cut-off voltage 0.7 V, the solution is transparent), 1.5 Mn + 1.5 Ti + 3 H solution after 5 cycles and after 50 cycles (cut-off voltage 0.7 V, the solution is turbid), and 1.5 Mn + 1.5 Ti + 3 H solution after 50 cycles (cut-off voltage 0.4 V, the solution is transparent). Therefore, to maintain the stability of the high-concentration electrolyte during cycling, one charge–discharge cycle with a cut-off voltage of 0.4 V was performed after every 50 cycles (with a cut-off voltage of 0.7 V).

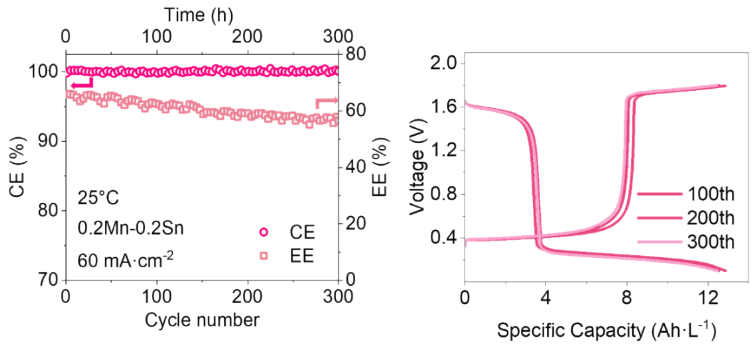

Figure S34. The cycling performance and charge-discharge curves of the flow battery with 0.2 Mn + 0.4 Ti + 3 H electrolyte at 60 mA·cm^{-2} with the discharge cutoff voltage of 0.1 V. It can be observed that after the discharge voltage cuts off at 0.1 V, a discharge plateau corresponding to the Ti^{4+}/Ti^{3+} redox couple appears, while the discharge capacity doubles. However, its cycling stability shows a slight decrease when compared to that with a discharge voltage cut-off at 0.4 V. Therefore, we choose to set the cut-off voltage at 0.4 V.

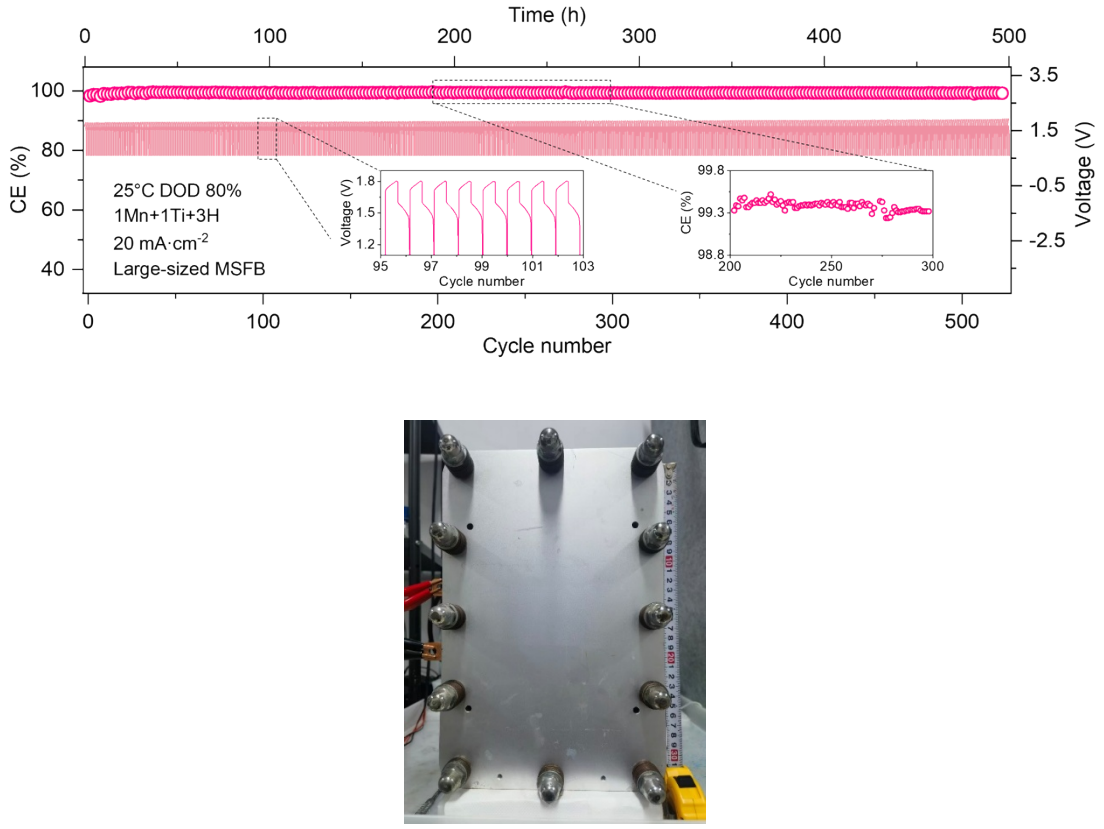

Figure S35. Large-sized battery with 1Mn+1Ti+3H electrolyte and N212 separator, showing its cycling performance and photos of the battery.

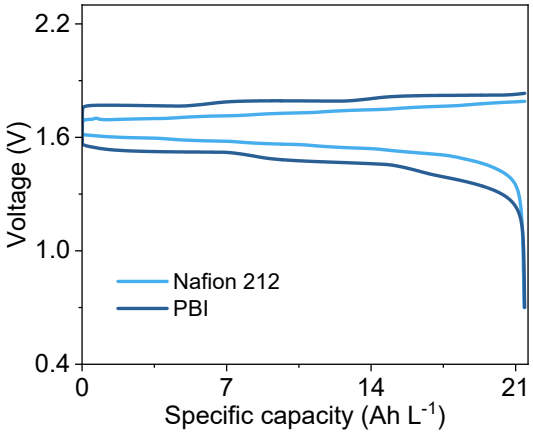

Figure S36. The charge-discharge curves of the batteries assembled with PBI membranes and Nafion 212 membranes at low temperature, respectively.

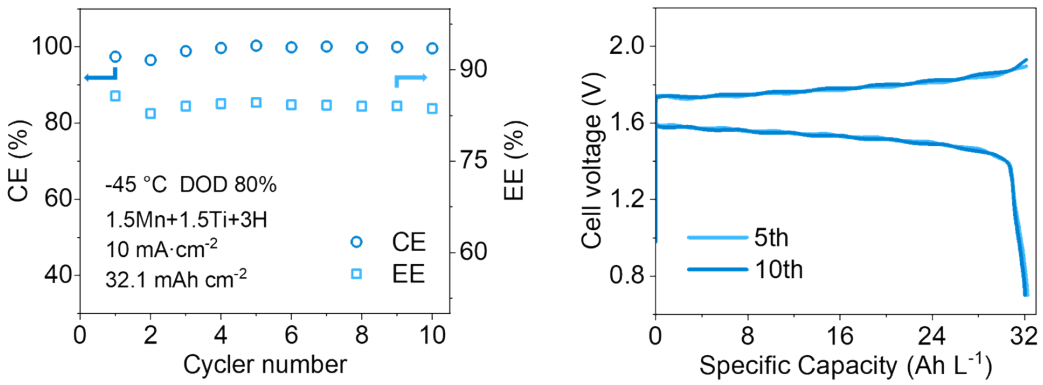

Figure S37. The cycling performance of the MSFB with high concentration electrolyte (1.5 Mn + 1.5 Ti + 3 H, DOD of 80%) at 10 mA·cm^{-2} under −45 °C. It can be seen that the flow battery is able to operate stably at −45 °C with high EE of 85%, and achieving a high energy density of 48 Wh L^{-1}.

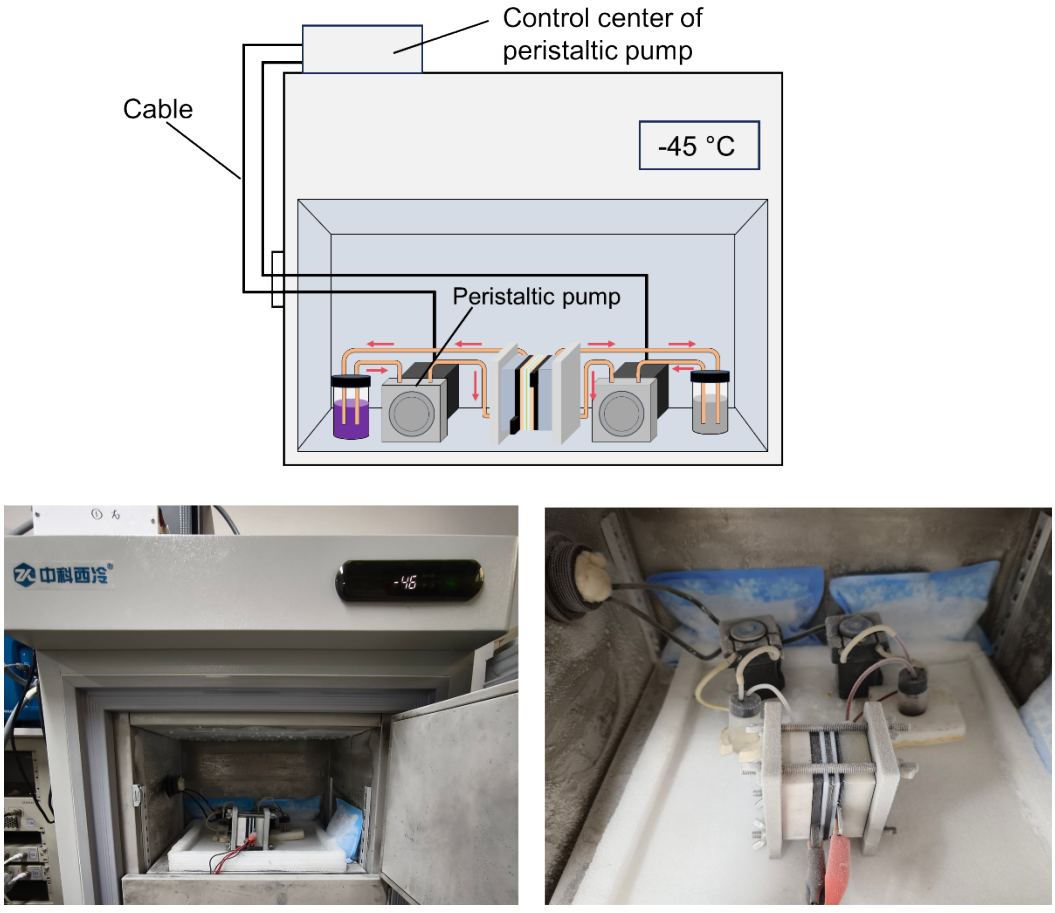

Figure S38. Schematic diagram and real-scene photos of the low-temperature testing device. (During the low-temperature battery test experiment, the peristaltic motor, the battery, and the electrolyte solution were all placed in the low-temperature box.)